Nuclear Instruments and Methods in Physics Research B 326 (2014) 298–302

Contents lists available at ScienceDirect

Nuclear Instruments and Methods in Physics Research B

journal homepage: www.elsevier.com/locate/nimb

Ion-irradiation induced reduction in $Sr_2Fe_{1.5}Mo_{0.5}O_{6-\delta}$ perovskite

Siwei Wang [a,b], Ming Tang [b,*], Kyle S. Brinkman [c], Fanglin (Frank) Chen [a]

[a] Department of Mechanical Engineering, University of South Carolina, Columbia, SC 29208, USA
[b] Materials Science and Technology Division, Los Alamos National Laboratory, Los Alamos, NM 87545, USA
[c] Science and Technology Directorate, Savannah River National Laboratory, Aiken, SC 29808, USA

ARTICLE INFO

Article history:
Received 16 July 2013
Received in revised form 11 September 2013
Accepted 2 October 2013
Available online 6 February 2014

Keywords:
Irradiation
Perovskite
Decomposition
Reduction
Amorphization

ABSTRACT

The incorporation of radioactive elements in fission products (FPs) into complex oxides, where the elements are constrained in the structure and enhanced leaching and radioactive stability can be obtained, is an active research area in the nuclear fuel cycle. Perovskite structured $Sr_2Fe_{1.5}Mo_{0.5}O_{6-\delta}$ (SFM) has the capability of incorporating several FPs (such as Sr and Mo) into the crystalline network simultaneously while maintaining a stabilized structure. The radiation damage effects on the structure changes of this polycrystalline SFM sample is conducted under various ion irradiations including 200 keV He ions to a fluence of 5×10^{20} ions m^{-2}, 100 keV H to a fluence of 3×10^{21} ions cm^{-2}, and 600 keV Kr ions to a fluence of 2.5×10^{19} ions m^{-2} at room temperature. Irradiation-induced structural evolution was examined by using grazing incidence X-ray diffraction and cross-sectional transmission electron microscopy. It was found that the irradiated SFM sample decomposed into a layered $Sr_4FeMoO_{8-\delta}$ based phase and a metallic Fe based phase under light ion (He and H) irradiations. Nano-crystallized secondary phase was observed with particle sizes around 7 nm. These results suggest that irradiation-induced reducing atmospheres may affect the stability of crystalline structure in complex oxides. Experiment results also reveal an amorphization in the heavy ion Kr irradiated sample, while no amorphization is observed in He/H irradiated SFM.

1. Introduction

The perovskites and related structured crystalline materials have been widely studied in many areas including dielectrics, ferromagnetics, superconductors and fuel cells [1–7]. One unique property of the perovskite is that it remains a stable structure within the tolerance factor t ranging from 0.78-1.05, where t is a description of degree of distortion and is defined as

$$t = (r_A + r_O)/2^{1/2}(r_B + r_O) \quad (1)$$

where r_A, r_B, and r_O are the ionic radii of A, B and O respectively for the perovskite with a formular of ABO_3. Due to such a large tolerance range, the perovskite structure can accommodate various elements into the crystalline network while maintaining its structure. Mo doped perovskite such as $Sr_2Fe_{1.5}Mo_{0.5}O_{6-\delta}$ (denoted as SFM afterwards) was previously investigated as magnetoresistive materials and solid oxide fuel cell electrode materials [8–10]. $Sr_2Fe_{1.5}Mo_{0.5}O_{6-\delta}$ is traditionally written as a double perovskite structure, where 1/4 of B sites are occupied by Mo. The crystal structure of SFM is *Fm-3m*, with lattice parameter $a = 7.8717$ Å (PDF#97-009-6223) [11]. While it has been later revealed that unlike other ordered double perovskites, the Mo and Fe atoms randomly occupy rather than orderly distribute in the B and B' sites, thus it is actually a simple perovskite structured oxide with proposed *Pm-3m* structure [12]. Recent detailed neutron diffraction study on SFM further suggests a *Pnma* structure and that the structure of this material is very sensitive to the concentration of oxygen vacancies [13].

Perovskite phases have also been proposed as possible ceramic host phases for the immobilization of actinides and some long-lived fission products (FP) including ^{90}Sr, Mo, and any of the lanthanides (Ln) (or alternatively, ^{99}Tc, and ^{137}Cs) [14,15]. The potential materials for immobilization of nuclear waste must be able to endure extreme radiation environment associated with α-decay of the actinides and β-decay of the fission products. In the previous studies, several research groups have performed ion beam irradiations on perovskite $SrTiO_3$ to study its radiation tolerance [16–20]. An irradiation-induced crystalline to amorphous phase transformation was observed on $SrTiO_3$, and quantitatively studies on the critical dose and temperature for amorphization were already reported [16,18,20]. The critical amorphization dose at room temperature is less than 2 displacements per atom (dpa) in those studies.

In this study, we are focusing on the irradiation effect on the perovskite SFM oxide material which simultaneously incorporates

* Corresponding author. Tel.: +1 505 665 1472; fax: +1 505 667 8021.
E-mail address: mtang@lanl.gov (M. Tang).

0168-583X/$ - see front matter © 2014 Elsevier B.V. All rights reserved.
http://dx.doi.org/10.1016/j.nimb.2013.10.093

Sr and Mo FPs into the crystalline structure. Different ion species irradiations were employed to evaluate the radiation tolerance of this compound. The radiation induced structural evolution, including the decomposition of the material and appearance of secondary phases, as well as amorphization has been characterized using various techniques including grazing incidence X-ray diffraction (GIXRD) and transmission electron microscopy (TEM).

2. Experimental

SFM powder was prepared by a modified Pechini method as reported previously [9,21,22]. The metal nitrates were titrated and dissolved stoichiometrically, where glycine and citric acid were used as chelating and complexing agents. The solution was then heated and combusted to ashes, followed by firing the as-prepared ash powder at 1000 °C for 5 h. The obtained ash powder grinded pressed into pellets to sinter at 1300 °C for 4 h. The as sintered pellets were cut into pieces and polished with alumina lapping films to obtain a mirror finish for further investigation. For the ion irradiation experiments, all samples were finally polished with a 40 nm colloidal silica slurry (Syton HT50, DuPont Air Products NanoMaterials L.L.C, Tempe, AZ), in order to remove the surface damage created by the previous mechanical polishing steps.

Ion irradiation experiments were performed at room temperature (~300 K) at the Ion Beam Materials Laboratory, Los Alamos National Laboratory, using a 200 kV Danfysik high current research ion implanter. 600 keV Kr^{+++}, 200 keV He^{++}, and 100 keV H^{+} ions were used in this study in order to assess the role of the effect of different ion masses on radiation damage response. The Stopping and Range of Ions in Matter (SRIM) program [23] was used to estimate the displacement damage in ion irradiated SFM. A threshold displacement energy of 40 eV (this is an arbitrary assumption) was used for all target elements. Fig. 1 shows the results of this simulation for SFM: the peak displacement damage doses are ~5 dpa at a fluence of 2.5×10^{19} Kr ions m^{-2}; 1.2 dpa at a fluence of 5×10^{20} He ions m^{-2}; and 0.8 dpa at a fluence of 3×10^{21} H ions m^{-2}.

Irradiated samples were characterized using grazing incidence X-ray diffraction (GIXRD), transmission electron microscopy (TEM). GIXRD measurements were made using a Bruker AXS D8 Advanced X-ray diffractometer, Cu Kα radiation, a graphite monochromator, θ–2θ geometry. The diffractometer was equipped with a Göebel mirror to achieve parallel beam diffraction optics. Irradiated samples were also prepared in cross-sectional geometries for TEM examination. The ion irradiation-induced microstructure evolution was examined using FEI Tecnai F30 electron microscope operating at 300 kV.

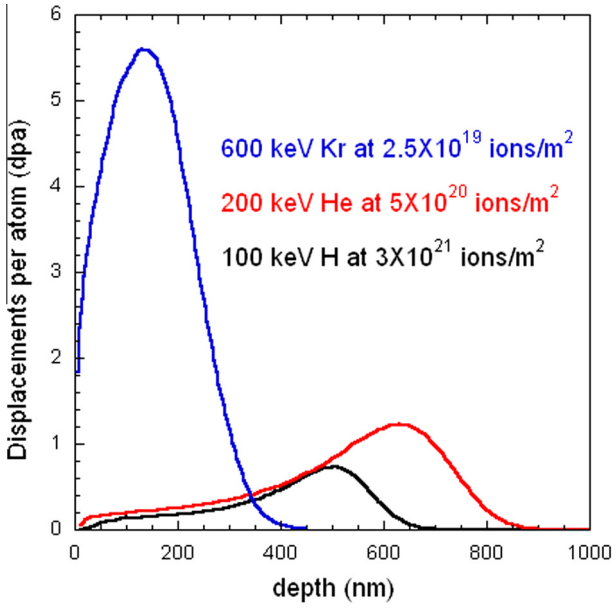

Fig. 1. SRIM simulation results for SFM under 100 keV H irradiation (Black line), 200 keV He irradiation (Red line) and 600 keV Kr irradiation (Blue line). (For interpretation of the references to color in this figure legend, the reader is referred to the web version of this article.)

3. Results and discussion

3.1. Ion irradiation induced reduction and phase decomposition

Fig. 2 shows GIXRD patterns obtained from SFM samples before and after 100 keV H and 200 keV He irradiations (Fig. 2(a) and (b)) at X-ray incidence angles $\alpha = 0.25°$ and 1°. Under these two X-ray incident angles, the calculated X-ray penetration depths fell with the predicted range of H ions (700 nm) and He ions (900 nm) into SFM target according to the SRIM calculations. Although we estimate X-ray penetration depth using both the critical angle formula [24] and the geometric method [25], it must be stated these are only estimation. XRD results reveal that the desired single phase perovskite SFM is obtained using the above fabrication method as shown in Fig. 2, denoted as pristine sample. The structure information has been reported in our previous publication, showing a cubic perovskite *Pm-3m* structure, with lattice parameter $a = 3.9287$ Å, which is equivalent to that of SFM with *Fm-3m* structure if transformed into a cubic double perovskite structure [12]. Irradiation induced a significant structural evolution in SFM, as observed from the GIXRD measurements. As shown in Fig. 2(a), from the patterns of the H irradiated samples, the additional peaks (other than the pristine SFM phase) can be identified as Fe (PDF#97-005-3451) and layered $Sr_4FeMoO_{8-\delta}$ (PDF#97-015-2243) based composites. It is interesting that SFM was decomposed and the Fe ions were reduced into metallic Fe based phase. It was reported that for metal oxides (binary oxides such a FeO, Fe_2O_3, CoO, TiO_2 and Nb_2O_5, etc.), the reduction in oxidation state caused by ion bombardment could be accounted for the preferential removal of oxygen and ion-induced oxide reduction [26–28]. Similarly, in our case, such kind of ion-induced reduction in oxidation state in perovskite structured SFM may be also due to the preferential sputtering of oxygen atoms from the oxide matrix. The mechanism can be understood through a collisional approach to explain the average composition of metal-to-oxygen concentration ratio [27], or a thermal approach to explain specific stoichiometries [28].

The pristine SFM sample powder was treated in reduced H_2 atmosphere at 900 °C for 10 h to compare with the H irradiated SFM sample. It can be seen from Fig. 2(a) that the XRD pattern of irradiated SFM is very similar to that of the reduced SFM. After H_2 reduction at high temperature, SFM decomposed and one of the reactions happened:

$$2Sr_2Fe_{1.5}Mo_{0.5}O_{6-\delta} = 2Fe + Sr_4FeMoO_{8-\delta} \quad (2)$$

The similar XRD spectra between the H_2 atmosphere and H irradiation experiments validate the hypothesis that the He irradiation may have resulted in a locally extremely reducing condition for the irradiated SFM sample. It should be noted that similar to $Sr_2Fe_{1.5}Mo_{0.5}O_{6-\delta}$ which deviated from $Sr_2FeMoO_{6-\delta}$ based composition, the decomposed $Sr_4FeMoO_{8-\delta}$ only represents the base secondary phase. In other words, the Fe/Mo ratio in the secondary phase is not determined to be 1:1, but is varied, and the Sr content is not necessarily 4. The decomposition of SFM also occurs with other possibilities such as a combination of an oxide with a parent perovskite [29]. As shown in Fig. 2(a), for the GIXRD patterns of the

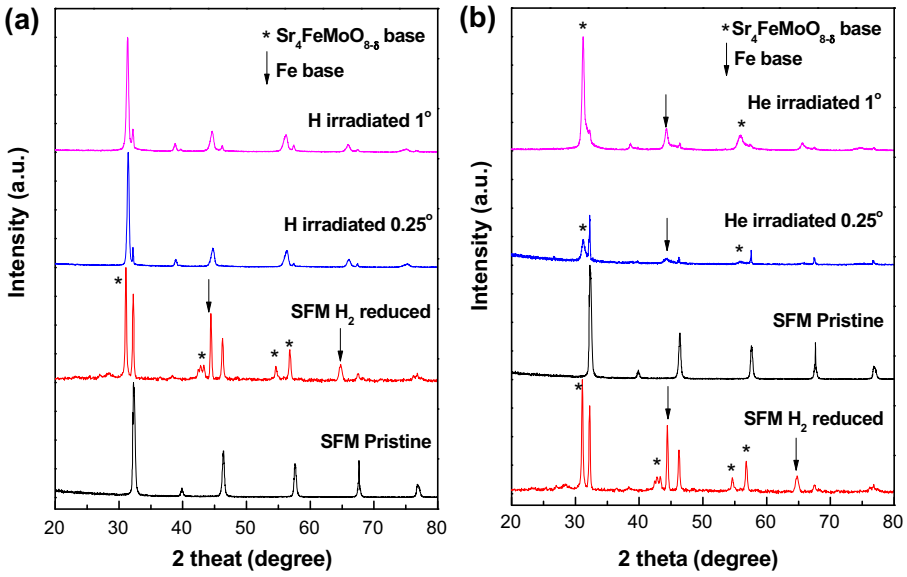

Fig. 2. (a) XRD patterns for pristine, H ion irradiated, and H_2 reduced SFM samples. (b) XRD patterns for pristine, He ion irradiated, and H_2 reduced SFM samples.

irradiated sample of incident angle 0.25° and 1°, the additional peaks become predominant over the SFM phase. This implies that most of SFM has been decomposed into secondary phases at these corresponding penetration depths (from very top surface to the peak dpa; and H distribution area) based on the SRIM calculations.

Metallic Fe based phase and the secondary phases have also been observed in SFM following 200 keV He irradiation. Fig. 2(b) shows the GIXRD results of SFM before and after 200 keV He irradiation at a fluence of 5×10^{20} He ions m^{-2}. New GIXRD reflections, other than those corresponding to the pristine SFM phase, are consistent with metallic Fe phase and the secondary phases. This observation suggests that He irradiation in SFM also induces reduction and decomposition.

As shown in Fig. 2(b), for the GIXRD patterns of the He ion irradiated sample, at incident angle of 0.25°, the additional peaks show up along with the peaks of the SFM phase, indicating that the content of the secondary phases are comparable with the SFM phase at this specific X-ray penetration depth (very top surface based on calculation). For incident angles from 1°, the secondary phases predominate over the SFM phase, implying that most of SFM has been decomposed into secondary phases at this corresponding penetration depth which is close to the peak dpa and He distribution area. This is in agreement with the SRIM calculation, where the irradiation is observed below 900 nm – a point where He ions preferentially knock off an oxygen, and the Fe ion is reduced to Fe metal [30].

Fig. 3 shows a cross-sectional TEM observation on 200 keV He irradiated SFM sample. From Fig. 3(a) the different morphologies for the unirradiated and irradiated layers can be clearly identified. The unirradiated substrate shows light gray background with smooth surface and some scratches due to the polishing treatment, while the ion irradiated damage layer shows dark gray color with coarsened morphology. The thickness of the ion irradiated damage layer is 800 ± 5 nm, consistent with the SRIM simulation result. Selected area electron diffraction (SAED) experiments were performed for the TEM sample with a probe size of 100 nm to examine the localized variation of lattice distortions along the irradiation path. Fig. 3(b) and (c) shows the corresponding SAED patterns along [−113] zone axis for the unirradiated SFM substrate and the irradiated damage layer, respectively. For the unirradiated substrate layer, the calculated d-spacing for the (220) peak is 0.2759 nm. While for the ion irradiated damage layer, from the SAED pattern shown in Fig. 3(c), the d-spacing for the (220) peak is around 0.2770 nm. The lattice parameter of the ion irradiated damage layer was expanded by 0.40%. Such SAED pattern in Fig. 4(c) may be caused by the appearance of the secondary $Sr_4FeMoO_{8-\delta}$ based phase with an ordered structure. For example, for ordered $Sr_4FeMoO_{8-\delta}$, the (110) peak is 0.2771 nm, very close to the value obtained from the observed SAED pattern. Further study to determine the stoichiometric composition of $Sr_4FeMoO_{8-\delta}$ and the Fe based content will be conducted.

Fig. 4 shows the high resolution TEM image of He ion irradiated damage layer. No irradiation-induced amorphization is observed for the irradiated sample. However, it can be clearly seen from Fig. 4 that sphere like nano-crystals are distributed uniformly in the ion irradiated damage layer with average grain size around 7 nm. It is difficult to determine from the TEM images what the exact structural information is for the nano-crystals, but it is determined that the nano-crystals are well crystallized, and the crystal structures of these nano-crystals are clearly different from the background lattices. The background lattice orientation and lattice parameter are consistent with the information obtained from XRD and SAED results that it is [−113] zone axis oriented.

3.2. Ion irradiation induced amorphization

Fig. 5 shows GIXRD patterns obtained from SFM samples before and after 600 keV Kr irradiation with a fluence of 2.5×10^{19} ions m^{-2} (corresponding to a peak dose of 5 dpa) at X-ray incidence angles $\alpha = 0.25°$, 0.5° and 1°. In Fig. 5, no additional peaks in Kr irradiated SFM as those in H/He irradiated SFM are observed. There is no peak shifting and broadening at incidence angle of 0.25° and 0.5°, where the calculated X-ray penetration depth is blow 100 nm. The result suggests that there is no observable structural evolution in the surface area of Kr irradiated SFM sample. However, an important observation is made at X-ray incidence angle of 1° scan, in that there is an apparent broad diffraction feature in the scattering angle $2\theta = 25–30°$, attributable to an amorphous structure. At the incidence angle of 1°, X-ray samples ~400 nm thick volume in the sample. These GIXRD measurements indicate that a phase transformation from crystalline to amorphous layer occurs in a deeper region of irradiated SFM, where the material

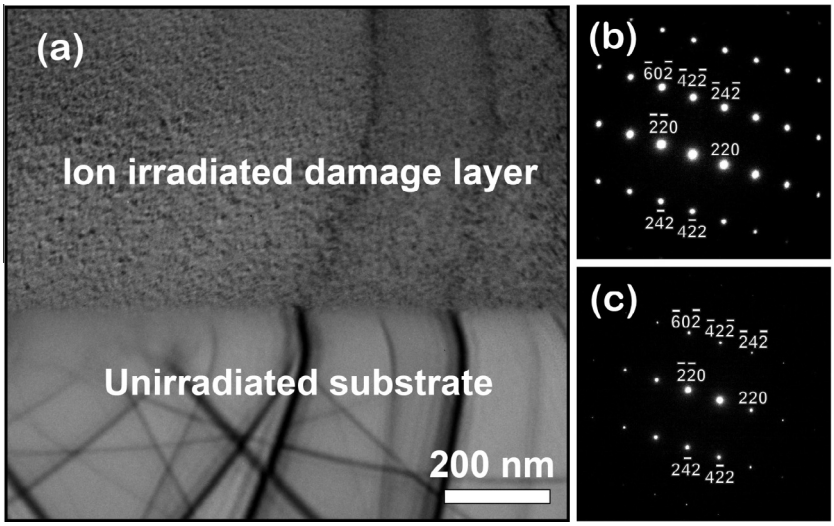

Fig. 3. (a) TEM image of the He ion irradiated SFM sample with unirradiated substrate and ion irradiated damage layer, (b) SAED pattern of unirradiated SFM substrate along the [−1 1 3] zone axis, and (c) SAED pattern of ion irradiated damage layer along the [−1 1 3] zone axis of the sample.

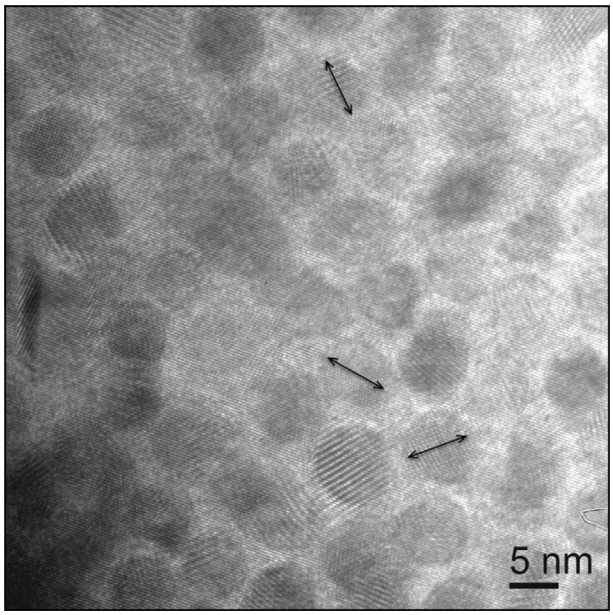

Fig. 4. HRTEM image corresponding to the [−1 1 3] zone axis of the irradiated SFM sample.

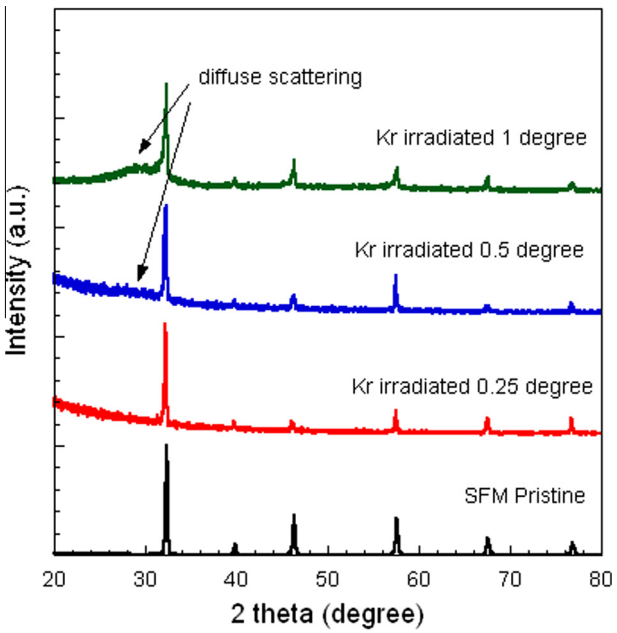

Fig. 5. GIXRD patterns for Kr ion irradiated sample with different incident angles.

experiences high ballistic damage fluence; whereas the surface region remaining crystalline occurs in a region where material experiences low ballistic damage fluence. The cumulative damage in the shallow region of the sample is smaller than that in the deep region (based on SRIM simulation in Fig. 1), so this explains why the amorphization appears with the increase of GIXRD grazing incidence angle. Here, we could estimate that the initiation of this amorphization occurs at a displacement damage dose over 4 dpa based on the damage depth profile calculated by SRIM.

3.3. Discussion

We report the decomposition and reduction of SFM ceramic into nano-crystals under light ion (including H and He) irradiations. Light ion irradiation preferentially sputtered oxygen atoms off the structure of SFM, reducing Fe ions into Fe metals, and the ramification of which is the formation of $Sr_4FeMoO_{8-\delta}$ based phase. Such decomposition and reduction led to the precipitation of nano-crystals with average sizes around 7 nm. The mechanism and results of the reduction process are analogous to the reduction of SFM in reducing atmospheres, where in both situations the oxygen atoms are taken off the structure. The equivalent "local" oxygen partial pressure the H/He ion irradiation provides should depend on the energy and fluence of the irradiation, while the decomposition of the material should depend on the oxygen partial pressure the H/He irradiation provides, the intensity of the ion beam bombardment, and the stability of the material itself. It further suggests that the H/He irradiation may provide a "locally" very reducing environment for the materials, and thus the stability in reducing atmospheres may be one critical criterion for searching potential nuclear waste form materials. In other words, if a material is chemically not stable in reducing atmospheres, it will probably suffer decomposition under energetic H/He ion irradiations.

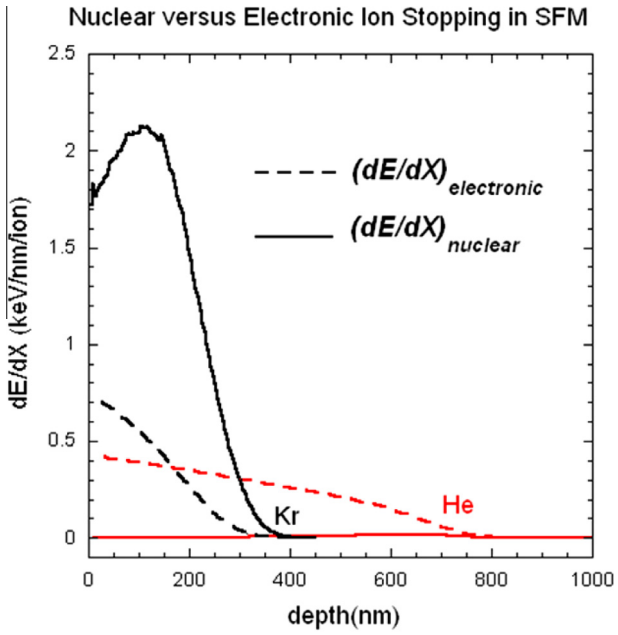

Fig. 6. Nuclear $(dE/dx)_{nuclear}$ versus electronic $(dE/dx)_{electronic}$ stopping in SFM for 200 keV He (Red in color) versus 600 keV Kr ions (Black in color), calculated using SRIM. (For interpretation of the references to color in this figure legend, the reader is referred to the web version of this article.)

Interestingly, heavy ion irradiation (600 keV Kr) does not induce the similar decomposition and reduction on SFM, even at higher displacement damage dose; although an amorphization occurs in Kr irradiated SFM. The difference in radiation response of SFM under light ions (H and He) versus heavy ion Kr irradiations suggests that an irradiation spectrum effect is influencing radiation effects. In other words, decomposition/reduction and amorphization in irradiated SFM exhibit sensitivity to irradiation spectrum. Fig. 6 shows nuclear $(dE/dx)_{nuclear}$ versus electronic $(dE/dx)_{electronic}$ stopping in SFM for 200 keV He versus 600 keV Kr ions, calculated using SRIM. It is clear that electronic stopping plays a greater role in the total stopping power for He versus Kr ions. However, notice that the magnitudes of the electronic stopping powers for He and Kr ions are not greatly different near the sample surface (the first 100 nm or so). Thus, it would be difficult to argue that the ionization is responsible for the differences in radiation response between He and Kr. The most noticeable difference between these two irradiation conditions is the nuclear energy density deposited per incident ion during stopping. Nuclear stopping power for 600 keV Kr ions exhibits a maximum of ~2 keV/nm/ion at a depth of 150 nm and is much greater than 0.05 keV/nm/ion throughout most of the range. On the contrary, nuclear stopping for 200 keV He ions is less than 0.05 keV/nm/ion over the entire ion range. This result implies that nuclear stopping power is responsible for the amorphization observed in Kr irradiated SFM.

A number of observations in this study are not fully understood at this time. For instance, the structural information for the nanocrystal grains in the He irradiated surface, as well as the different amorphization dose dependence between structurally similar materials $SrTiO_3$ and $Sr_3Ti_2O_7$ are not fully understood. Work is currently in progress to explore ion irradiation effects on SFM in more details.

5. Conclusion

The irradiation effect on $Sr_2Fe_{1.5}Mo_{0.5}O_{6-\delta}$ perovskite structured oxide ceramic has been evaluated. GIXRD measurements and TEM observations on SFM compounds reveal two ion irradiation-induced phenomena: first, 100 keV H and 200 keV He ion irradiations decompose SFM into metallic Fe and layered structured $Sr_4FeMoO_{8-\delta}$ based phase, leaving a nano-crystalized structured morphology, but no such decomposition observed in 600 keV Kr irradiated SFM; second, amorphization is observed in Kr irradiated SFM, while no irradiation-induced amorphization is observed in SFM under H and He irradiations at room temperature. These results suggest that a potential criterion applied for radiation tolerance of nuclear wastes or advanced nuclear fuel forms, is the structural stability of the materials in locally reducing atmospheres arising from fission product decay in the crystalline matrix.

Acknowledgements

The financial supports from the US Department of Energy, Office of Nuclear Energy's Fuel Cycle Research & Development (FCR&D) programs and Nuclear Energy University Programs (NEUP) are gratefully acknowledged. SW would also like to thank the Seaborg Institute Summer Fellowship program sponsored by the Seaborg Institute for Transactinium Science, Los Alamos National Laboratory.

References

[1] N. Erdman, K.R. Poeppelmeler, M. Asta, O. Warschkow, D.E. Ellis, L.D. Marks, Nature (London) 419 (2002) 55.
[2] F. Prado, L. Mogni, G.J. Cuello, A. Caneiro, Solid State Ionics 178 (2007) 77.
[3] Y.G. Ko, W.Y. Lee, Catal. Lett. 83 (2002) 157.
[4] G.D. Wilk, R.M. Wallace, J.M. Anthony, J. Appl. Phys. 89 (2001) 5243.
[5] B. Schupp, K. Dorr, K. Ruck, K. Nenkov, K.H. Muller, G. Krabbes, Solid State Sci. 7 (2003) 17.
[6] K. Oyoshi, S. Hishita, H. Haneda, J. Appl. Phys. 87 (2000) 3450.
[7] M. Kiyotoshi, E. Kazuhiro, Appl. Phys. Lett. 67 (1995) 2468.
[8] T. Yamamoto, J. Liimatainen, J. Linden, M. Karppinen, H. Yamauchi, J. Mater. Chem. 10 (2000) 2342.
[9] G. Xiao, Q. Liu, S. Wang, V.G. Komvokis, M.D. Amiridis, A. Heyden, S. Ma, F. Chen, J. Power Sources 202 (2012) 63.
[10] Q. Liu, X. Dong, G. Xiao, F. Zhao, F. Chen, Adv. Mater. 22 (2010) 5478.
[11] G. Liu, G. Rao, X. Feng, H. Yang, Z. Ouyang, W. Liu, J. Liang, J. Alloys Compd. 353 (2003) 42.
[12] Q. Liu, D.E. Bugaris, G. Xiao, M. Chmara, S. Ma, H.-C. zur Loye, M.D. Amiridis, F. Chen, J. Power Sources 196 (2011) 9148.
[13] A.B. Muñoz-García, D.E. Bugaris, M. Pavone, J.P. Hodges, A. Huq, F. Chen, H.-C. zur Loye, E.A. Carter, J. Am. Chem. Soc. 134 (2012) 6826.
[14] W.J. Weber, R.C. Ewing, C.R.A. Catlow, T. Diaz de la Rubia, L.W. Hobbs, C. Kinoshita, Hj. Matzke, A.T. Motta, M. Nastasi, E.K.H. Salje, E.R. Vance, S.J. Zinkle, J. Mater. Res. 13 (1998) 1434.
[15] A.E. Ringwood, S.E. Kesson, K.D. Reeve, D.M. Levins, E.J. Ramm, Radioactive Waste Forms for the Future, in: W. Lutze, R.C. Ewing (Eds.), North-Holland, Amsterdam, 1988, p. 233.
[16] A. Meldrum, L.A. Boatner, R.C. Ewing, Nucl. Instrum. Methods Phys. Res. Sec. B 141 (1998) 347.
[17] C. Sabathier, J. Chaumont, J.-C. Krupa, Nucl. Instrum. Methods Phys. Res. Sec. B 196 (2002) 308.
[18] Y. Zhang, J. Lian, C.M. Wang, W. Jiang, R.C. Ewing, W.J. Weber, Phys. Rev. B 72 (2005) 094112.
[19] Y. Zhang, C.M. Wang, M.H. Engelhard, W.J. Weber, J. Appl. Phys. 100 (2006) 113533.
[20] Y. Zhang, J. Lian, Z. Zhu, W.D. Bennett, L.V. Saraf, J.L. Rausch, C.A. Hendricks, R.C. Ewing, W.J. Weber, J. Nucl. Mater. 389 (2009) 303.
[21] S. Wang, F. Zhao, L. Zhang, F. Chen, Solid State Ionics 213 (2012) 29.
[22] S. Wang, F. Zhao, L. Zhang, K. Brinkman, F. Chen, J. Alloys Compd. 506 (2010) 263.
[23] J.F. Ziegler, J.P. Biersack, U. Littmark, The Stopping and Range of Ions in Solids, Pergamon Press, New York, 1985.
[24] A. Guinier, X-Ray Diffraction in Crystals Imperfect Crystals and Amorphous Bodies, Dover Publications Inc, New York, 1994.
[25] D. Rafaja, V. Valvoda, A.J. Perry, J.R. Treglio, Surf. Coat. Technol. 92 (1997) 135.
[26] T. Choudhury, S.O. Saied, J.L. Sullivan, A.M. Abbot, J. Phys. D Appl. Phys. 22 (1989) 1185.
[27] J.B. Malherbe, S. Hofmann, J.M. Sanz, Appl. Surf. Sci. 27 (1986) 355.
[28] R. Kelly, Surf. Sci. 100 (1980) 85.
[29] M.M. Kuklja, E.A. Kotomin, R. Merkle, Y.A. Mastrikov, J. Maier, Phys. Chem. Chem. Phys. 15 (2013) 5443.
[30] S. Wang, M. Tang, L. Zhang, G. Xiao, K.S. Brinkman, F. Chen, J. Alloys Compd. 578 (2013) 170.